PRAMANA
— journal of
physics

Vol. 65, No. 3
September 2005
pp. 437–455

The shape of an axisymmetric bubble in uniform motion

P N SHANKAR
33/1 Kasturba Road Cross, Bangalore 560 001, India
E-mail: pn_shankar55@rediffmail.com

MS received 21 March 2005; accepted 23 May 2005

Abstract. We consider in a frame fixed to a bubble translating with steady speed U, the inviscid, axisymmetric, irrotational motion of the liquid past it. If all speeds are normalized by U and lengths by $T/\frac{1}{2}\varrho U^2$, where T is the surface tension of the liquid–bubble interface, it can be shown that the unknown bubble shape and field depend on a single parameter $\Gamma = (p_\mathrm{b} - p_\infty)/\frac{1}{2}\varrho U^2 - 1$ alone, where the pressures are the ones in the bubble and far away respectively. When Γ is very large the bubble is almost spherical in shape while for $\Gamma \leq \Gamma^* \approx -0.315$, bubbles whose exteriors are simply connected do not exist. We solve the non-linear, free boundary problem for the whole range $\Gamma^* < \Gamma < \infty$ by the use of an analytical representation for the bubble shape, a surface singularity method to compute potential flows and a generalized Newton's method to continue in Γ. Apart from providing explicit representations for bubble shapes and detailed numerical values for the bubble parameters, we show that the classical linearized solution for large Γ is a very good approximation, surprisingly, to as low values of Γ as 2. We also show that Miksis *et al* [1] is inaccurate over the whole range and in serious error for large and small Γ. These have been corrected.

Keywords. Axisymmetric bubble shapes; non-linear free boundary problems; surface singularity methods in potential flows.

PACS Nos 47.55.Dz; 47.11.+j; 47.15.Hg

1. Introduction

Consider a bubble rising in a pure liquid. The forces on the bubble that determine its motion are the buoyancy acting upwards and the viscous drag in opposition. When these are in balance the bubble will move upwards with uniform velocity, the terminal velocity U. Let r_e be the equivalent radius of the bubble, i.e., the radius of a spherical bubble of the same volume as that of the bubble, let ϱ and μ be the liquid density and viscosity respectively and T be the surface tension of the liquid–bubble interface. Then the relevant dimensionless parameters governing the steady motion can be shown to be

$$\mathrm{M} = g\mu^4/\varrho T^3, \tag{1a}$$

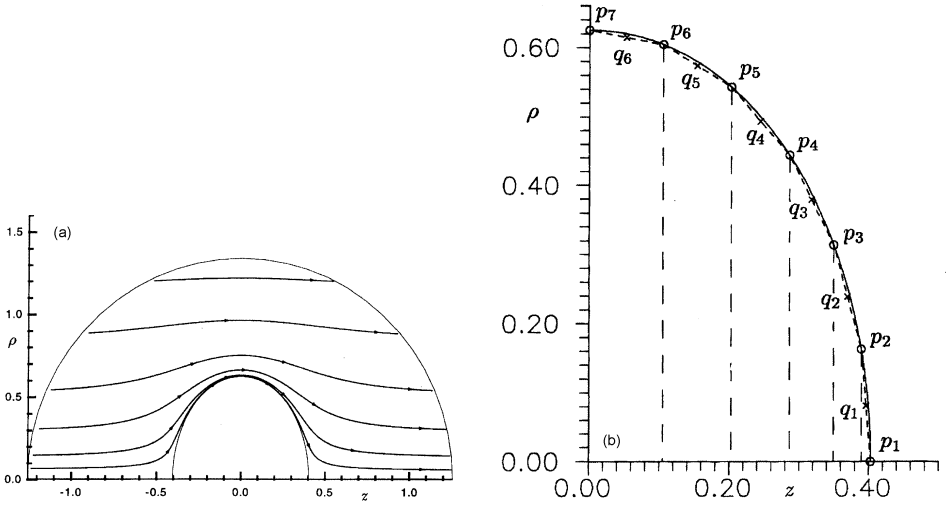

Figure 1. Uniform inviscid flow past an axisymmetric bubble. (**a**) Streamlines in the meridional plane, (**b**) the type of panelling used to compute the potential flow past the bubble. $\Gamma = 2$.

$$\mathrm{Re} = 2r_{\mathrm{e}}U\varrho/\mu, \tag{1b}$$

$$\mathrm{W} = 2r_{\mathrm{e}}U^2\varrho/T, \tag{1c}$$

where M, Re and W are the Morton number, the Reynolds number and the Weber number respectively. We note that M depends on the liquid properties alone. The extensive experiments of Haberman and Morton [2] showed that the nature of the bubble shape and motion depended critically on M. These matters are discussed in some detail in Moore [3]. The reader interested in knowing more about the variety of experimentally observed phenomena may also consult Clift *et al* [4] and Bhaga and Weber [5]. A review of recent progress made in describing bubble motion in inhomogeneous flow is given in Magnaudet and Eames [6]. Here, however, we shall only be concerned with bubbles in steady, rectilinear motion with no separation and weak wakes.

It is an interesting fact that, provided the Reynolds number Re is high enough, as it often is, this uniform motion can be treated to a good approximation as inviscid [3,7,8]. That is, even though viscosity plays an essential role in achieving this motion, it can be neglected when studying the steady terminal state. In fact, as shown by Levich [9], even the drag on the bubble can be well-estimated by calculating the dissipation in the fluid using the *inviscid* field to estimate it. As a consequence the computation of inviscid bubble motion is of considerable practical interest in addition to its obvious theoretical importance.

When studying the uniform motion of a bubble, it is convenient to work in a frame moving with the bubble in which case we consider the steady, irrotational motion of the inviscid fluid past the stationary bubble. The problem then reduces to finding the potential Φ that leads to a uniform flow at infinity, a velocity field that has no normal component on the bubble surface Σ and a pressure field that

satisfies the Laplace–Young capillarity jump condition on Σ. Let us assume the bubble and the fluid field to be axisymmetric; it will be convenient to use cylindrical polar coordinates (ρ, φ, z), where the field will be independent of φ. Figure 1a then shows how the streamlines past a typical bubble will look like in a meridional plane. Let U be the steady bubble speed and let p_∞ and p_b be the pressures at infinity and inside the bubble respectively. We normalize all speeds by U and lengths by $T/\frac{1}{2}\varrho U^2$. It can then be checked that the field then depends on a single parameter Γ, $\Gamma = (p_\mathrm{b} - p_\infty)/\frac{1}{2}\varrho U^2 - 1$, alone. Thus the problem amounts to finding a Φ which leads to a velocity field $(0, 0, 1)$ at infinity, no normal velocity on Σ such that the pressure jump condition on Σ which, as a consequence of Bernoulli's equation, takes the form

$$\overline{q}^2 = K - \Gamma \tag{2}$$

is satisfied. In (2) $\overline{q}$ is the liquid speed on Σ and K is the dimensionless curvature of the bubble surface. It is to be noted that Σ is not known and has to be determined as part of the solution. One can therefore think of the problem as one where, given the parameter Γ, the shape of the bubble is to be determined.

Although the general problem of finding the bubble shape is difficult as it is a non-linear, free boundary problem, the limit $\Gamma \to \infty$ is readily understood. We observe that when $U \to 0$, that is, when the bubble is almost stationary, it must be nearly spherical in shape. Thus from eq. (2) we conclude that for $\Gamma \to \infty$, $K \to \Gamma$. Having this limiting solution it is natural to seek a perturbation about this and this was obtained by Moore [3] who showed that to the next order of approximation the bubble would be an oblate ellipsoid. Some more sophisticated efforts were also made [3,10,11] and although these do appear to improve the estimates of the drag coefficient of the bubble, they do not seem to improve the estimation of the bubble shape. The fact is that as the bubble speeds up or as Γ decreases the bubble shape undergoes distortions that do not permit it to be accurately represented as an ellipsoid of known dimensions. The bubble's aspect ratio increases until at $\Gamma = 0$ its meridional profile resembles that of a straight sided cigar. As Γ decreases further the bubble begins to develop negative curvature near the z-axis, which increases in magnitude with further decreases in the parameter, until at *pinch-off*, when $\Gamma = \Gamma^*$, the fore and aft sides of the bubble touch at the axis. Beyond this, presumably, the bubble can exist only as a toroidal bubble; this is the idealized picture since, depending on the values of M, Re and W, a variety of instabilities can lead to unsteady motions and shape changes well before $\Gamma = \Gamma^*$.

A number of papers have appeared [12–14] in which inviscid bubble shapes over a part of the range of Γ have been computed. Since their major objectives lay elsewhere, however, their computations were limited. To the best knowledge of the present author the only paper that has attempted to deal, over the whole range $\Gamma^* < \Gamma < \infty$, with inviscid bubble shapes and related parameters as its main objective is Miksis *et al* [1] (which will hereafter be referred to as MVK). Reformulating the problem as an integral equation on the (unknown) bubble boundary alone, discretization leads them to a system of non-linear algebraic equations which they solve by Newton's method. Apart from determining various important bubble parameters as functions of Γ, they present, graphically, the bubble shapes for six values of Γ ranging from 50 to -0.251, the closest they get to pinch-off.

The present investigation was initiated for two reasons. In an earlier investigation of plane bubbles [15] an exact solution had been found for the case $\Gamma = 0$. One wondered whether some simplification occurred in the axisymmetric case too for that special value of the parameter. Second, in none of the works cited is the bubble shape given analytically; thus anyone wishing to know the actual bubble shape for some arbitrary value of Γ would have difficulty in even estimating it from the published literature. Our results have also lead us to the conclusion that there are serious, hitherto undetected errors in MVK. We will try to explain the reasons for the discrepancy between their results and ours.

The very simple method used in this investigation is outlined in §2, the surprisingly interesting results for large Γ are discussed in §3, bubbles with negative curvature and those close to pinch-off are described in §4 while overall bubble parameters are considered in §5.

2. A computational procedure to determine bubble shapes

Ideally, we would like a computational procedure that has the following features: (a) the bubble shapes should be described analytically, (b) the potential flow calculation should be fast and reasonably accurate, (c) the iterative procedure for determining the shape should be rugged and (d) we should be able to make an estimate of the errors involved in the computation. In trying to meet these requirements the following procedure was devised.

When choosing an analytical representation for the bubble shape we must make sure that: (i) it can handle shapes with negative curvature, (ii) as a consequence of fore-aft symmetry the bubble profile slope must vanish for $z = 0$, (iii) the slope must be infinite for $\rho = 0$ and (iv) it should use a small number of coefficients. It was found that a representation that satisfies all these conditions is a conformal mapping of a circle of initially unknown radius R in an auxilliary complex plane $\zeta = te^{i\phi}$. We write

$$z + i\rho = \zeta + \sum_{l=1}^{\infty} \frac{R^{2l}\gamma_l}{\zeta^{2l-1}}, \tag{3}$$

where γ_l are real scalars that have to be determined. Then on the circle $t = R$ we have

$$\rho = R\left(\sin\phi - \sum_{l=1}^{\infty} \gamma_l \sin(2l-1)\phi\right), \tag{4a}$$

$$z = R\left(\cos\phi + \sum_{l=1}^{\infty} \gamma_l \cos(2l-1)\phi\right). \tag{4b}$$

In actual practice the bubble shape is represented only by a finite number, $m-1$, of terms in the above sums so that the total number of unknowns including R is m. It is found that m can be as small as 2 or 3 for large Γ with very good accuracy while near pinch-off m may need to be as large as 25 for the same accuracy or less.

We observe that unlike in the plane case [15] this representation does not lead to an especially easy resolution of the potential problem.

A reasonably fast and accurate method for computing potential flows about arbitrary bodies is the surface singularity or panel method due to Hess and Smith [16]. The axisymmetric case, which is of relevance to us, is based on the field due to an axisymmetric ring source of unit strength and radius ρ_0. If it is centered at $z = z_0$ the induced velocity field $(V_\rho, 0, V_z)$ can be shown to be given by

$$V_\rho = \frac{2\rho_0}{\rho\sqrt{[(\rho+\rho_0)^2+(z-z_0)^2]}}\left[K(\lambda)+\frac{\rho^2-\rho_0^2-(z-z_0)^2}{(\rho-\rho_0)^2+(z-z_0)^2}E(\lambda)\right], \tag{5a}$$

$$V_z = \frac{4\rho_0(z-z_0)E(\lambda)}{[(\rho-\rho_0)^2+(z-z_0)^2]\sqrt{[(\rho+\rho_0)^2+(z-z_0)^2]}}, \tag{5b}$$

$$\lambda = \frac{4\rho_0\rho}{(\rho+\rho_0)^2+(z-z_0)^2}, \tag{5c}$$

where $K(\lambda)$ and $E(\lambda)$ are complete elliptic integrals of the first and second kind, respectively. The idea then is to represent the axisymmetric bubble by $2n$ panels on each of which are uniformly distributed sources of the type (5) with initially unknown source strengths σ_j. If the bubble is represented by (4), choose $2n+1$ equally spaced points on the semi-circle $\zeta = R\mathrm{e}^{i\phi}, 0 \le \phi \le \pi$. Neighbouring points are joined by straight-line segments. This leads to an approximation of the bubble surface by the inclined surfaces of $2n$ frustums of cones. This type of panelling is illustrated in figure 1b where $n = 6$, $p_1p_2, p_2p_3, ...$ are the panel surfaces and $q_1, q_2, ...$ are the control points at the centres of the panels. On each panel are distributed the uniform ring sources of strength $\sigma_j, j = 1, 2, ..., 2n$. These $2n$ source strengths are determined by demanding that, with uniform unit flow at infinity, the normal velocity vanish at the $2n$ control points q_j. In our case some simplification occurs since we have fore-aft symmetry. Although the full bubble has to be panelled, only n unknowns have to be determined as $\sigma_j = -\sigma_{2n-j+1}$. For more details on the method, especially about the self-induction on any panel, one can refer to [16].

The iterative procedure for determining the bubble shape for a given Γ employs a generalized Newton's method. An initial approximation for the bubble shape is chosen, i.e., an initial approximation $R, \gamma_l, l = 1, 2, ..., m$ is chosen. Now we employ $2km = 2n$ panels on the bubble surface when computing the potential flow around the bubble, i.e., there are k, $k \ge 1$, panels for each unknown in the bubble shape. Once the flow past the candidate bubble shape is determined we can compute the errors made ϵ_j, $j = 1, 2, ..., n$ (on half the bubble) in the satisfaction of the capillarity pressure jump condition (2)

$$\epsilon_j = \overline{q_j}^2 - K_j + \Gamma, \quad j = 1, 2, ..., n. \tag{6}$$

Note that the curvatures K_j are evaluated at points on the bubble surface adjacent to the control points q_j. We then define the m cumulative errors squared

$$e_l^2 = \sum_{j=1}^{k} \epsilon_{k(l-1)+j}^2, \quad l = 1, 2, ..., m \tag{7}$$

which will be used in Newton's method. Note that all that has been done is that m groups of k contiguous panels each have been generated and on each group e_l^2 is the total error squared. While there is some freedom in its choice, in the present work k was at least 5 for large Γs and was as much as 30 for bubbles near pinch-off. Note also that the root mean squared error on the $2n$ panels, $\overline{e}$, is just given by

$$\overline{e} = \sqrt{\sum_{l=1}^{m} e_l^2}. \tag{8}$$

In order to employ Newton's method, we make small incremental changes $\delta R, \delta\gamma_l$ in turn of R and each γ_l and determine the generalized gradient $\partial e_l^2/\partial R, \partial e_l^2/\partial\gamma_j$. Newton's method then leads to changes $\mathrm{d}R, \mathrm{d}\gamma_l$ that have to be made to diminish the errors e_l. One then iterates in the usual manner, except that here for given m and k the errors can only be minimized rather than driven to zero. This in outline is the procedure.

Now for some details that may be of interest. The formula that we employ to compute the curvature is identical to the one used by MVK. If the bubble profile in a meridional plane is given by $z = \eta(\rho)$, the curvature takes the form

$$K = K_1 + K_2 = -\frac{\eta''}{(1+\eta'^2)^{3/2}} - \frac{\eta'}{\rho(1+\eta'^2)^{1/2}}, \tag{9}$$

where K_1 is the principal curvature obtained by treating the profile as a plane curve while K_2 is the other associated principal curvature; K_2 can be deduced geometrically from the curvature ρ^{-1} of the axisymmetric ring at that z-plane. It can be verified that the above formula is valid for all possible bubble shapes including ones with negative curvature [17].

In assessing the accuracy of the present approach it must be kept in mind that, although the limit $\Gamma \to \infty$ is well-understood, the exact bubble shape is not known for any Γ. Here we will try to provide an estimate by estimating the errors in the two components that contribute to the total error: the error in the calculation of the potential flow and the error in satisfying condition (2) on Σ. Table 1 shows the maximum percentage error and the rms percentage error in the surface tangential velocity component as functions of n, the number of panels used for half the sphere,

Table 1. The maximum percentage error and the root mean square percentage error in the computations for a sphere as functions of the number of panels used.

Number of panels	Maximum percentage error	Root mean square percentage error
50	0.32885	0.16988
100	0.19266	0.08736
200	0.13374	0.04369
300	0.12967	0.03039
450	0.34273	0.02561
600	0.55121	0.27070

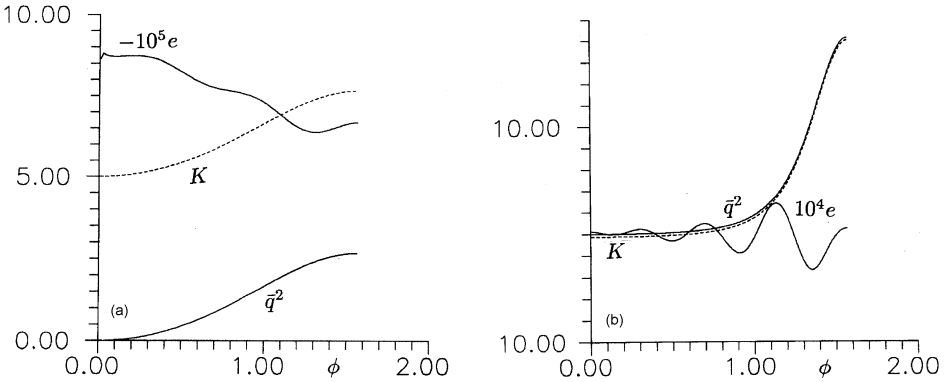

Figure 2. The distribution of the error, $e = \bar{q}^2 - K + \Gamma$, over the bubble surface. (**a**) $\Gamma = 5$, $m = 5$, $n = 100$, (**b**) $\Gamma = -0.25$, $m = 10$, $n = 300$.

for potential flow past a sphere. As one might expect, increasing n leads, at least in this range, to better accuracy and although these are for a sphere there is every reason to expect that this holds in the case of bubble shapes. Figure 2 shows the distribution over the bubble surface of e, the error in satisfying (2), and the curvature and the square of the surface speed for two values of Γ. We remark that (2) implies that $K - \bar{q}^2 = \text{constant} = \Gamma$ on Σ and the figures, with two parallel curves each, show how well this is achieved by the computations.

3. The limit $\Gamma \to \infty$ and bubble shapes of non-negative curvature for $\Gamma \geq 0$

Before we discuss the results of the present study we compare our results with those of MVK. Miksis *et al* [1] plot bubble shapes for six values of Γ and in figure 3a we have compared our shapes with theirs for all those six values [19]. It must be pointed out that for every one of the cases considered in figure 3a, at least two curves from our calculations for different computational parameters (m, n) have been plotted. For the first four cases the two are indistinguishable while in the fifth, one can be barely separately made out; it is only in the last case that the inaccurate solution can be clearly made out near the neck but even in this case the shapes are indistinguishable near the top. This is to emphasize that many checks have been made to confirm the consistency of the present calculations.

Now coming to MVK's data, excluding the case $\Gamma = 50$, a superficial assessment may lead to the conclusion that the agreement is satisfactory. However, keeping in mind that we are comparing two numerical computations of steady, potential flow, we must consider this to be poor agreement even for these five cases; this is especially true since we are dealing with bubble *shapes* where the curvature is very sensitive to small errors in shape. Going back to the case $\Gamma = 50$ the matter is even more serious since here one has no choice but to admit that there is disagreement: at least one of the computations is in serious error. It may be of interest that this case was considered last as the limit $\Gamma \to \infty$ is the easy limit and good agreement

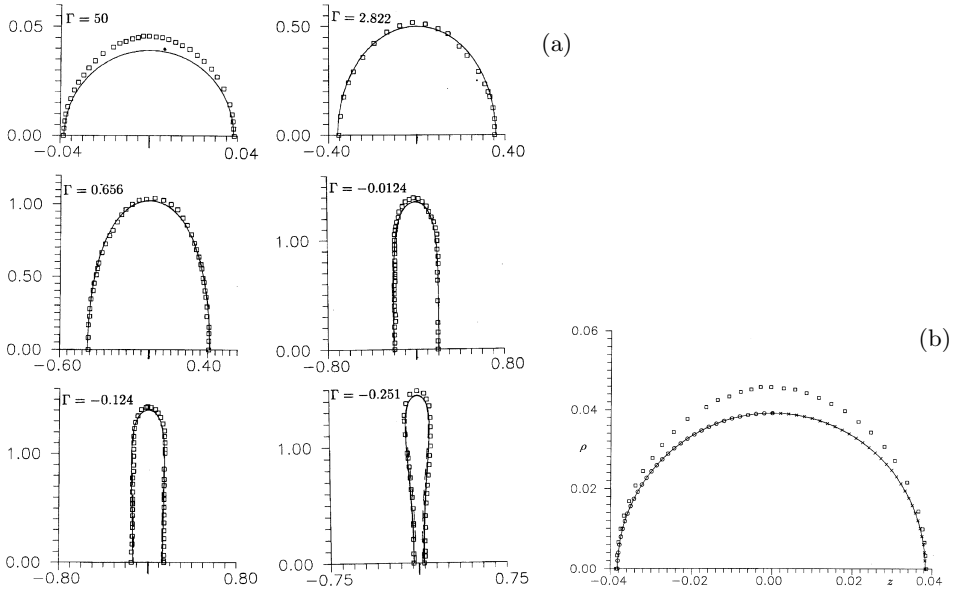

Figure 3. (**a**) Comparison of the bubble profiles obtained by Miksis *et al* [1] (□) with those obtained by the present method (- - -, —). (**b**) Comparison of the bubble profile obtained by Miksis *et al* [1] for $\Gamma = 50$ (□) with those resulting from three different calculations. (—) Conformal mapping and surface singularity method, (×) conformal mapping and multipole expansion method, (○) the $r = \Sigma_l \alpha_l \cos 2l\theta$ and multipole expansion method.

was expected. We have carefully checked all our procedures and calculations and have reluctantly come to the conclusion that MVK are in error. In support of this conclusion the following need to be pointed out:

(a) MVK's calculations do not agree with the theoretical, small perturbation results of Moore [3] for large Γ while the present ones do. This will be discussed in greater detail below.

(b) In order to demonstrate that there is nothing special about the method used in this paper we have redone the calculation for $\Gamma = 50$, the critical case, using different methods for computing the potential flow and describing the bubble shape. For the potential one can use a multipole expansion

$$\Phi(r, \phi, \theta) = r\cos\theta + \sum_{i=1}^{\infty} \beta_i \frac{P_{2i-1}(\cos\theta)}{r^{2i}}, \tag{10}$$

where P_i are the Legendré polynomials, n terms in the sum are taken and β_i are determined by the normal velocity condition. For the bubble shape one can take

$$r = \mathcal{R}(\theta) = \alpha_0 + \alpha_1 \cos 2\theta + \alpha_2 \cos 4\theta + \cdots = \sum_{l=0}^{m-1} \alpha_l \cos 2l\theta \tag{11}$$

which has the right behaviour for $\theta = 0, \pi/2$ and determine the coefficients α_l. Note

that this representation cannot be used for bubbles which neck on the axis as r is multivalued in θ in these cases.

First, the multipole expansion (10) with $n = 5$ was used to determine the coefficients in the conformal mapping representation (4) with $m = 5$. It was found that $R \approx 0.03869, \gamma_1 \approx -0.01113, \gamma_2 \approx -0.34 \times 10^{-5}$, with the other two much smaller. These numbers compare very favourably with those in table 2, derived using the surface singularity method. Next, the multipole expansion was used to determine the coefficients in the representation (11) for the shape. We find $\alpha_0 \approx 0.03868, \alpha_1 \approx -0.43 \times 10^{-3}, \alpha_2 \approx 0.35 \times 10^{-5}$ and the others much smaller. The resulting bubble shapes are shown in figure 3b, where for the latter two results, only points on half the bubble each are shown for clarity. We note that the three quite different calculations agree very well amongst themselves but the MVK profile is significantly off.

(c) Apart from some numerical data which apparently support their claim that their calculations are 'very nearly second-order accurate', MVK provide no estimates of the errors in their calculations. In the absence of exact solutions to compare with, we have tried to provide some estimates of the errors by giving the known errors in the potential calculation for flow past a sphere (table 1) and by providing the rms error in satisfying condition (2), $\bar{e}$, for every calculation that has been carried out. Table 2 lists the mapping coefficients $R, \gamma_l, l = 1, 2, ..., m$ for a range of Γs from 1000 to near pinch-off and for every one of these cases the rms error is listed.

(d) As in most, if not all, other previous bubble calculations MVK do not provide bubble shapes analytically and as a consequence checking becomes difficult. In table 2 we provide the bubble shapes analytically and it should be very easy to check whether these are accurate solutions or not. In our opinion this is the strength of the present technique.

Although we are not in a position to determine the source of inaccuracy or error in MVK, figure 3a does suggest a possible source. One notes that the best cases in the figure are for $\Gamma = 2.822$ and $\Gamma = 0.656$: matters become worse for both large Γ and for $\Gamma \to \Gamma^*$. It is to be noted that in both the latter cases the curvature K becomes large over a considerable part of the bubble. It is our guess that MVK's procedure has difficulty in handling large curvatures; a corollary is that they would have great difficulty in computing for really large values of Γ, whereas as table 2 testifies we have no such difficulty. An explanation of why MVK's errors have remained undetected for so long is postponed to §5.

The first matter of interest when looking at convex bubbles is the limit $\Gamma \to \infty$ when the bubbles are almost spherical in shape. Of considerable help here is the linearized theory of Moore [3]. As the bubble is spherical in that limit, Moore naturally considers a perturbation about this shape. Assuming that the bubble will be an ellipsoid of revolution and using the pressure field on the associated sphere for enforcing the pressure jump condition (2), he was able to show, for large Γ that the bubble aspect ratio, $\chi = b/a$, and the Weber number, W, given by (1c) are linearly related

$$\chi = b/a = 1 + \frac{9}{64}\mathrm{W}. \tag{12}$$

Table 2. The mapping coefficients that determine the bubble shape as a function of Γ. For each Γ the first number is R and the following numbers are the γ, in sequence. Thus for $\Gamma = 1000$, $R \approx 0.200E-02$, $\gamma_1 \approx -0.561E-03$ and $\gamma_2 \approx -0.885E-8$.

$\Gamma = 1000.00$	$m = 3$	$n = 90$	$\bar{e} = 0.673\text{E}-02$	.
$0.199665\text{E}-02$	$-0.561113\text{E}-03$	$-0.884511\text{E}-08$		
$\Gamma = 100.00$	$m = 5$	$n = 100$	$\bar{e} = 0.141\text{E}-03$	
$0.196678\text{E}-01$	$-0.558487\text{E}-02$	$-0.811699\text{E}-06$	$0.319699\text{E}-07$	$0.125283\text{E}-07$
$\Gamma = 90.00$	$m = 5$	$n = 50$	$\bar{e} = 0.383\text{E}-03$	
$0.218134\text{E}-01$	$-0.619067\text{E}-02$	$-0.100255\text{E}-05$	$0.571296\text{E}-07$	$0.835480\text{E}-08$
$\Gamma = 80.00$	$m = 5$	$n = 50$	$\bar{e} = 0.424\text{E}-03$	
$0.244836\text{E}-01$	$-0.695935\text{E}-02$	$-0.128371\text{E}-05$	$0.577146\text{E}-07$	$0.169046\text{E}-07$
$\Gamma = 70.00$	$m = 5$	$n = 50$	$\bar{e} = 0.478\text{E}-03$	
$0.278987\text{E}-01$	$-0.794646\text{E}-02$	$-0.181541\text{E}-05$	$0.384510\text{E}-08$	$-0.140709\text{E}-09$
$\Gamma = 60.00$	$m = 5$	$n = 50$	$\bar{e} = 0.376\text{E}-03$	
$0.324206\text{E}-01$	$-0.925814\text{E}-02$	$-0.247487\text{E}-05$	$0.632878\text{E}-08$	$-0.866064\text{E}-10$
$\Gamma = 50.00$	$m = 5$	$n = 50$	$\bar{e} = 0.468\text{E}-03$	
$0.386915\text{E}-01$	$-0.110928\text{E}-01$	$-0.353532\text{E}-05$	$0.103875\text{E}-07$	$-0.179240\text{E}-08$
$\Gamma = 40.00$	$m = 5$	$n = 50$	$\bar{e} = 0.237\text{E}-03$	
$0.479687\text{E}-01$	$-0.138257\text{E}-01$	$-0.557156\text{E}-05$	$0.216129\text{E}-07$	$-0.273019\text{E}-09$
$\Gamma = 30.00$	$m = 5$	$n = 50$	$\bar{e} = 0.138\text{E}-03$	
$0.630960\text{E}-01$	$-0.183521\text{E}-01$	$-0.992067\text{E}-05$	$0.512288\text{E}-07$	$-0.494033\text{E}-09$
$\Gamma = 20.00$	$m = 5$	$n = 50$	$\bar{e} = 0.392\text{E}-03$	
$0.921413\text{E}-01$	$-0.272824\text{E}-01$	$-0.223770\text{E}-04$	$0.169958\text{E}-06$	$-0.164758\text{E}-08$
$\Gamma = 10.00$	$m = 5$	$n = 50$	$\bar{e} = 0.303\text{E}-03$	
$0.170524+00$	$-0.531173\text{E}-01$	$-0.898304\text{E}-04$	$0.126373\text{E}-05$	$-0.177912\text{E}-07$
$\Gamma = 9.00$	$m = 5$	$n = 100$	$\bar{e} = 0.452\text{E}-04$	
$0.186281\text{E}+00$	$-0.587716\text{E}-01$	$-0.110671\text{E}-03$	$0.171135\text{E}-05$	$-0.252249\text{E}-07$
$\Gamma = 8.00$	$m = 5$	$n = 100$	$\bar{e} = 0.438\text{E}-04$	
$0.205284\text{E}+00$	$-0.656271\text{E}-01$	$-0.140035\text{E}-03$	$0.238274\text{E}-05$	$-0.386846\text{E}-07$
$\Gamma = 7.00$	$m = 5$	$n = 100$	$\bar{e} = 0.904\text{E}-04$	
$0.228559\text{E}+00$	$-0.742864\text{E}-01$	$-0.182734\text{E}-03$	$0.345441\text{E}-05$	$-0.624212\text{E}-07$
$\Gamma = 6.00$	$m = 5$	$n = 100$	$\bar{e} = 0.585\text{E}-04$	
$0.257710\text{E}+00$	$-0.855702\text{E}-01$	$-0.248177\text{E}-03$	$0.527454\text{E}-05$	$-0.107322\text{E}-06$
$\Gamma = 5.00$	$m = 5$	$n = 100$	$\bar{e} = 0.766\text{E}-04$	
$0.295218\text{E}+00$	$-0.100872\text{E}+00$	$-0.355624\text{E}-03$	$0.861972\text{E}-05$	$-0.200535\text{E}-06$
$\Gamma = 4.00$	$m = 5$	$n = 100$	$\bar{e} = 0.993\text{E}-04$	
$0.345131\text{E}+00$	$-0.122782\text{E}+00$	$-0.549652\text{E}-03$	$0.154620\text{E}-04$	$-0.418598\text{E}-06$
$\Gamma = 3.00$	$m = 5$	$n = 100$	$\bar{e} = 0.694\text{E}-04$	
$0.414361\text{E}+00$	$-0.156685\text{E}+00$	$-0.952230\text{E}-03$	$0.317313\text{E}-04$	$-0.102068\text{E}-05$
$\Gamma = 2.00$	$m = 5$	$n = 100$	$\bar{e} = 0.924\text{E}-04$	
$0.514951\text{E}+00$	$-0.215744\text{E}+00$	$-0.199183\text{E}-02$	$0.800529\text{E}-04$	$-0.312144\text{E}-05$

Table 2. *Continued.*

$\Gamma = 1.50$	$m = 5$	$n = 100$	$\bar{e} = 0.385\text{E} - 04$	
0.582544E+00	$-0.264986\text{E} + 00$	$-0.323567\text{E} - 02$	$0.142843\text{E} - 03$	$-0.639185\text{E} - 05$
$\Gamma = 1.00$	$m = 5$	$n = 100$	$\bar{e} = 0.919\text{E} - 04$	
0.663170E+00	$-0.341212\text{E} + 00$	$-0.593928\text{E} - 02$	$0.281264\text{E} - 03$	$-0.136144\text{E} - 04$
$\Gamma = 0.80$	$m = 5$	$n = 100$	$\bar{e} = 0.111\text{E} - 03$	
0.699140E+00	$-0.384216\text{E} - 00$	$-0.792944\text{E} - 02$	$0.379013\text{E} - 03$	$-0.194523\text{E} - 04$
$\Gamma = 0.60$	$m = 5$	$n = 100$	$\bar{e} = 0.179\text{E} - 03$	
0.734668E+00	$-0.437994\text{E} + 00$	$-0.109402\text{E} - 01$	$0.517161\text{E} - 03$	$-0.258569\text{E} - 04$
$\Gamma = 0.40$	$m = 5$	$n = 100$	$\bar{e} = 0.192\text{E} - 03$	
0.767785E+00	$-0.506266\text{E} + 00$	$-0.156341\text{E} - 01$	$0.700028\text{E} - 03$	$-0.368206\text{E} - 04$
$\Gamma = 0.20$	$m = 5$	$n = 100$	$\bar{e} = 0.348\text{E} - 03$	
0.794259E+00	$-0.593592\text{E} + 00$	$-0.232058\text{E} - 01$	$0.921791\text{E} - 03$	$-0.416850\text{E} - 04$
$\Gamma = 0.00$	$m = 10$	$n = 300$	$\bar{e} = 0.611\text{E} - 04$	
0.807107E+00	$-0.703490\text{E} + 00$	$-0.356039\text{E} - 01$	$0.103315\text{E} - 02$	$-0.427270\text{E} - 04$
$0.237621\text{E} - 05$	$-0.156849\text{E} - 06$	$0.254515\text{E} - 07$	$-0.882099\text{E} - 08$	$0.171072\text{E} - 08$
$\Gamma = -0.05$	$m = 10$	$n = 300$	$\bar{e} = 0.840\text{E} - 04$	
0.807525E+00	$-0.735233\text{E} + 00$	$-0.397402\text{E} - 01$	$0.102409\text{E} - 02$	$-0.399242\text{E} - 04$
$0.253092\text{E} - 05$	$0.655860\text{E} - 09$	$0.476965\text{E} - 07$	$0.355689\text{E} - 07$	$0.187454\text{E} - 07$
$\Gamma = -0.10$	$m = 10$	$n = 300$	$\bar{e} = 0.871\text{E} - 04$	
0.806519E+00	$-0.768692\text{E} + 00$	$-0.443982\text{E} - 01$	$0.984846\text{E} - 03$	$-0.353909\text{E} - 04$
$0.291053\text{E} - 05$	$0.133107\text{E} - 06$	$0.477754\text{E} - 07$	$0.830837\text{E} - 07$	$0.439479\text{E} - 08$
$\Gamma = -0.15$	$m = 10$	$n = 300$	$\bar{e} = 0.718\text{E} - 04$	
0.803965E+00	$-0.804001\text{E} + 00$	$-0.496313\text{E} - 01$	$0.909656\text{E} - 03$	$-0.271391\text{E} - 04$
$0.436399\text{E} - 05$	$0.245060\text{E} - 06$	$0.990063\text{E} - 07$	$0.440906\text{E} - 08$	$-0.342803\text{E} - 08$
$\Gamma = -0.20$	$m = 10$	$n = 300$	$\bar{e} = 0.454\text{E} - 04$	
0.799677E+00	$-0.841375\text{E} + 00$	$-0.555558\text{E} - 01$	$0.785389\text{E} - 03$	$-0.971613\text{E} - 05$
$0.929734\text{E} - 05$	$0.157502\text{E} - 05$	$0.361067\text{E} - 06$	$0.744066\text{E} - 07$	$0.176805\text{E} - 07$
$\Gamma = -0.25$	$m = 15$	$n = 300$	$\bar{e} = 0.302\text{E} - 03$	
0.793145E+00	$-0.882856\text{E} + 00$	$-0.626323\text{E} - 01$	$0.585244\text{E} - 03$	$0.372340\text{E} - 04$
$0.307771\text{E} - 04$	$0.101388\text{E} - 04$	$0.333704\text{E} - 05$	$0.110300\text{E} - 05$	$0.347021\text{E} - 06$
$0.828322\text{E} - 07$	$0.340971\text{E} - 07$	$-0.117871\text{E} - 07$	$0.560236\text{E} - 08$	$-0.492583\text{E} - 08$
$\Gamma = -0.26$	$m = 15$	$n = 300$	$\bar{e} = 0.446\text{E} - 03$	
0.790786E+00	$-0.895547\text{E} + 00$	$-0.649559\text{E} - 01$	$0.491936\text{E} - 03$	$0.629820\text{E} - 04$
$0.483658\text{E} - 04$	$0.188889\text{E} - 04$	$0.707812\text{E} - 05$	$0.261425\text{E} - 05$	$0.895889\text{E} - 06$
$0.266994\text{E} - 06$	$0.105404\text{E} - 06$	$-0.584146\text{E} - 08$	$0.132558\text{E} - 07$	$-0.883687\text{E} - 08$
$\Gamma = -0.27$	$m = 15$	$n = 300$	$\bar{e} = 0.192\text{E} - 03$	
0.789907E+00	$-0.900149\text{E} + 00$	$-0.658375\text{E} - 01$	$0.442902\text{E} - 03$	$0.709434\text{E} - 04$
$0.570499\text{E} - 04$	$0.235958\text{E} - 04$	$0.972906\text{E} - 05$	$0.372994\text{E} - 05$	$0.129835\text{E} - 05$
$0.503138\text{E} - 06$	$0.122996\text{E} - 06$	$0.964792\text{E} - 08$	$0.335964\text{E} - 07$	$-0.216711\text{E} - 07$
$\Gamma = -0.28$	$m = 20$	$n = 600$	$\bar{e} = 0.785\text{E} - 02$	
$0.788752\text{E} + 00$	$-0.905825\text{E} + 00$	$-0.673316\text{E} - 01$	$0.101164\text{E} - 03$	$-0.304525\text{E} - 04$
$0.238465\text{E} - 04$	$0.980878\text{E} - 05$	$-0.959995\text{E} - 05$	$-0.136672\text{E} - 04$	$-0.116825\text{E} - 04$
$-0.389101\text{E} - 05$	$0.561126\text{E} - 05$	$0.102784\text{E} - 04$	$0.115316\text{E} - 04$	$0.921236\text{E} - 05$
$0.665464\text{E} - 05$	$0.375368\text{E} - 05$	$0.250440\text{E} - 05$	$0.115753\text{E} - 05$	$0.771175\text{E} - 06$

Table 2. *Continued.*

$\Gamma = -0.29$	$m = 20$	$n = 600$	$\bar{e} = 0.111\text{E} - 02$	
$0.787604\text{E} + 00$	$-0.913577\text{E} + 00$	$-0.686899\text{E} - 01$	$0.136729\text{E} - 03$	$0.303463\text{E} - 04$
$0.594825\text{E} - 04$	$0.353707\text{E} - 04$	$0.190466\text{E} - 04$	$0.100104\text{E} - 04$	$0.417471\text{E} - 05$
$0.185580\text{E} - 05$	$0.731050\text{E} - 06$	$0.713726\text{E} - 07$	$-0.192501\text{E} - 06$	$-0.258599\text{E} - 06$
$-0.193791\text{E} - 06$	$-0.201000\text{E} - 06$	$-0.357059\text{E} - 07$	$0.272965\text{E} - 08$	$-0.148619\text{E} - 06$
$\Gamma = -0.30$	$m = 20$	$n = 600$	$\bar{e} = 0.663\text{E} - 02$	
$0.786170\text{E} + 00$	$-0.922114\text{E} + 00$	$-0.702284\text{E} - 01$	$0.127905\text{E} - 03$	$0.839444\text{E} - 04$
$0.969786\text{E} - 04$	$0.640926\text{E} - 04$	$0.462467\text{E} - 04$	$0.301538\text{E} - 04$	$0.183651\text{E} - 04$
$0.623817\text{E} - 05$	$-0.305111\text{E} - 05$	$-0.781211\text{E} - 05$	$-0.956747\text{E} - 05$	$-0.778502\text{E} - 05$
$-0.582115\text{E} - 05$	$-0.322453\text{E} - 05$	$-0.211108\text{E} - 05$	$-0.917844\text{E} - 06$	$-0.935126\text{E} - 06$
$\Gamma = -0.31$	$m = 25$	$n = 600$	$\bar{e} = 0.979\text{E} - 02$	
$0.784973\text{E} + 00$	$-0.928157\text{E} + 00$	$-0.703309\text{E} - 01$	$0.100746\text{E} - 02$	$0.715561\text{E} - 03$
$0.489897\text{E} - 03$	$0.298998\text{E} - 03$	$0.170265\text{E} - 03$	$0.920797\text{E} - 04$	$0.424007\text{E} - 04$
$0.150134\text{E} - 04$	$-0.171764\text{E} - 05$	$-0.980658\text{E} - 05$	$-0.137160\text{E} - 04$	$-0.153046\text{E} - 04$
$-0.143849\text{E} - 04$	$-0.133084\text{E} - 04$	$-0.111889\text{E} - 04$	$-0.908100\text{E} - 05$	$-0.702348\text{E} - 05$
$-0.503717\text{E} - 05$	$-0.353032\text{E} - 05$	$-0.240812\text{E} - 05$	$-0.132923\text{E} - 05$	$-0.102629\text{E} - 05$

Here, and in all that follows, a is the stream-wise dimension of the bubble along the z-axis while b is the lateral dimension in the plane $z = 0$. Thus Moore was able to show that his assumption on the shape was consistent with an oblate ellipsoid whose oblateness was explicitly related to the departure of W from W = 0 (or $\Gamma = \infty$). It would be natural to seek the next correction to $O(W^2)$ but Moore [3] was well aware of the difficulties involved and instead chose an approximate method first suggested by Hartunian and Sears [7]. By assuming the bubble to be oblate ellipsoidal for all values of χ and now satisfying the pressure jump condition at only two points, namely at the nose and the equator, he derived a relation between W and χ

$$\mathrm{W}(\chi) = 4\chi^{-4/3}(\chi^3 + \chi - 2)[\chi^2 \sec^{-1}\chi - (\chi^2 - 1)^{1/2}]^2(\chi^2 - 1)^{-3}. \quad (13)$$

It should be pointed out that, whereas (12) has a very sound basis as regular perturbation theory with transfer of boundary conditions is now classical, (13) has much less justification. In any case, figure 4 compares the present calculations with Moore's formulae (12) and (13); note that $\mathrm{W} \to 8\Gamma^{-1}$ as $\mathrm{W} \to 0$ and this has been used over the whole range. There is, as expected, excellent agreement between (12) and the numerical calculations. What is surprising is that the agreement is good to as low values of Γ as $\Gamma = 2$, at least as far as χ is concerned. Under these circumstances the discrepancy of the MVK result for $\Gamma = 50$, also shown in figure 4, is hard to understand [20]. Figure 4 also shows that (13) is a poor approximation except in that limit, $\Gamma^{-1} \to 0$, where (12) is in any case an excellent approximation. It is therefore surprising that in [1,11,14,21] (12) is virtually ignored while (13) is so extensively cited. In our opinion this is because the linear theory (12) does not 'predict' a maximum Weber number while (13) does.

Bubble shapes for non-negative values of Γ are shown in figure 5. Even for as low a value of Γ as 20 the bubble looks nearly spherical. As Γ is reduced a, b and χ all increase initially; however, around $\Gamma = 1.1$, a reaches a maximum of about 0.435 and begins to decrease monotonically from then on while b and χ continue

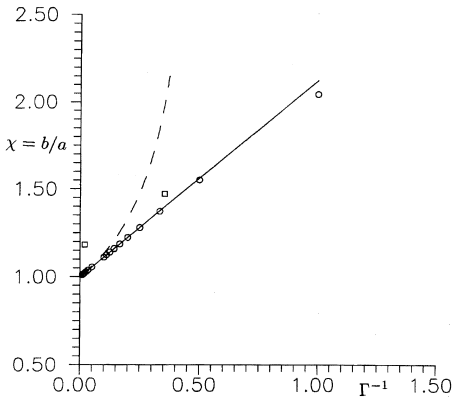

Figure 4. The limit $\Gamma \to \infty$. (—) Moore's linearized theory, eq. (12), (- - -) Moore's 'two-point' theory, eq. (13), (□) MVK's calculations, (○) present calculations.

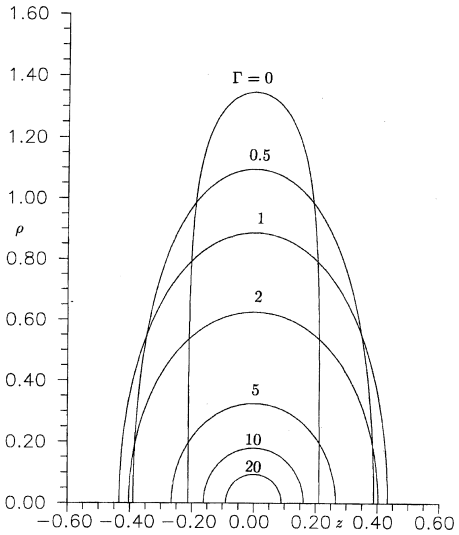

Figure 5. Bubble shapes of non-negative curvature for non-negative Γ.

to increase. As noted above, for $\Gamma < 2$ the shape increasingly departs from that of an ellipsoid of revolution. This can also be seen from table 2, where γ_2 and γ_3 begin to increase in magnitude. From the figure it can be seen that for $\Gamma = 0$ the sectional shape resembles that of a cigar with straight sides. One of the original motivations for the present study was to see whether one could obtain an 'exact' representation for the bubble shape for this value of Γ as had been possible in the plane case [15,22]. Examination of the mapping coefficients in this case (see table 2) did not suggest any obvious simplification. It is of course possible that simplification may occur with some other representation, but we did not pursue this matter any further.

4. Bubbles with negative curvature and the limit $\Gamma \to \Gamma^*$

We observe from the pressure jump condition (2) that at the fore and aft stagnation points the curvature must equal Γ. Thus as Γ becomes negative the curvature at these points must become negative and at least locally the shape will have to be concave. In fact, as Γ becomes more and more negative the concavity on the axis increases while the region of negative curvature spreads. This can be clearly seen in figure 6: with decreasing Γ the bubble begins to neck on the axis even as the lateral dimension b keeps increasing. One then expects that at some negative Γ^* the bubble will pinch-off, i.e. the opposite sides will touch and such axisymmetric shapes will not exist for lower Γs.

The need for increasing n as pinch-off is approached is demonstrated in figure 7, which shows how a decreases as Γ becomes increasingly negative. From this figure

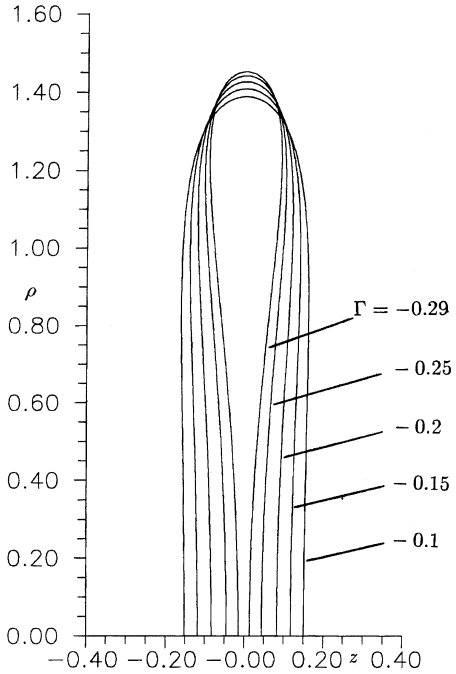

Figure 6. Bubble shapes with negative curvature for negative Γ.

we estimate $\Gamma^* \approx -0.315$, not very different from the value of -0.31 estimated by MVK, whose calculation nearest to pinch-off was for $\Gamma = -0.251$. Figure 8 shows bubble shapes and streamline patterns very close to pinch-off.

5. Discussion

Once the bubble shape is known one can easily determine a number of associated geometrical and dynamical parameters. In figure 9 are shown how the bubble dimensions a and b vary with Γ for $\Gamma^* < \Gamma \leq 4$. Whereas the lateral dimension increases monotonically with decreasing Γ, the stream-wise dimension initially increases, reaches a maximum around $\Gamma = 1.1$ and then decreases until it vanishes at pinch-off. The variation of the bubble surface area $\mathcal{S}$ and volume $\mathcal{V}$ are shown in figure 9b. Again the surface area increases monotonically with decreasing Γ while the volume exhibits a maximum of about 2.223 at $\Gamma \approx 0.24$.

The added mass $\mathcal{M}$, for translation in the z-direction, is a parameter of dynamical interest as it is a measure of how much of the fluid is actually affected by the motion of the bubble. A convenient formula for our use ([23], p. 103) is

$$\mathcal{M} = -\int_{\Sigma} \Phi' n_z \mathrm{d}\Sigma, \tag{14}$$

where Φ' is the disturbance potential due to the surface singularities and n_z is the

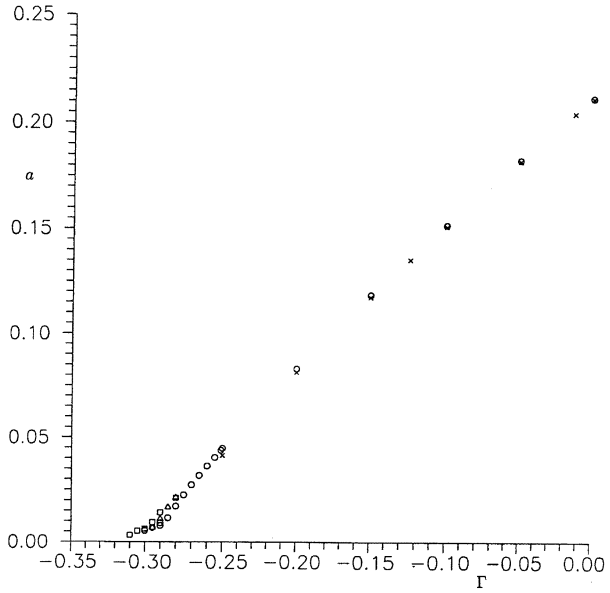

Figure 7. The decrease of a, the bubble half-width on the z-axis, with decreasing negative Γ. ($\times$) $n = 200$, ($\circ$) $n = 300$, ($\triangle$) $n = 450$, ($\square$) $n = 600$.

component of the unit normal in the z-direction; note that $\mathcal{M}$ is dimensionless. As a check, formula (14) and the panel calculation of the potential were used to find the added mass of an ellipsoid as a function of χ; our calculations were in agreement with the curve in figure 4.8 of Newman [24]. For the bubble, figure 9b shows that $\mathcal{M}$ increases monotonically with decreasing Γ all the way to pinch-off. By and large our results for the bubble parameters are similar to those displayed by MVK in their figures 3 and 4 although if examined carefully numerical differences are likely in view of the errors in their bubble shapes.

Finally, we come to the dependence of the Weber number on χ, a relationship which has traditionally been considered important and which, in the opinion of this writer, has lead to much confusion. A short calculation shows that

$$\mathrm{W} = 2(6\mathcal{V}/\pi)^{1/3} \tag{15}$$

and so we can expect a behaviour very similar to that of the volume, i.e., we can expect a maximum value although because of the small exponent the peak will not be as sharp. On the W–χ plot our results agree well with those of MVK and El Sawi [21] while Moore's two-point approximation, though yielding a maximum does poorly. We find a maximum Weber number, $\mathrm{W_c} \approx 3.239$, at $\chi \approx 3.832$ which compares well with 3.23 at 3.85 deduced by MVK. Moore [11] first pointed out that a maximum Weber number in the above plot suggested that there was a critical Weber number $\mathrm{W_c}$ beyond which the symmetric shape is impossible; moreover he remarked that for a given W less than the maximum the more distorted shape was probably unstable and would not occur in practice [25]. Although these observations are logical, it should be pointed out that calculations that differ considerably in the

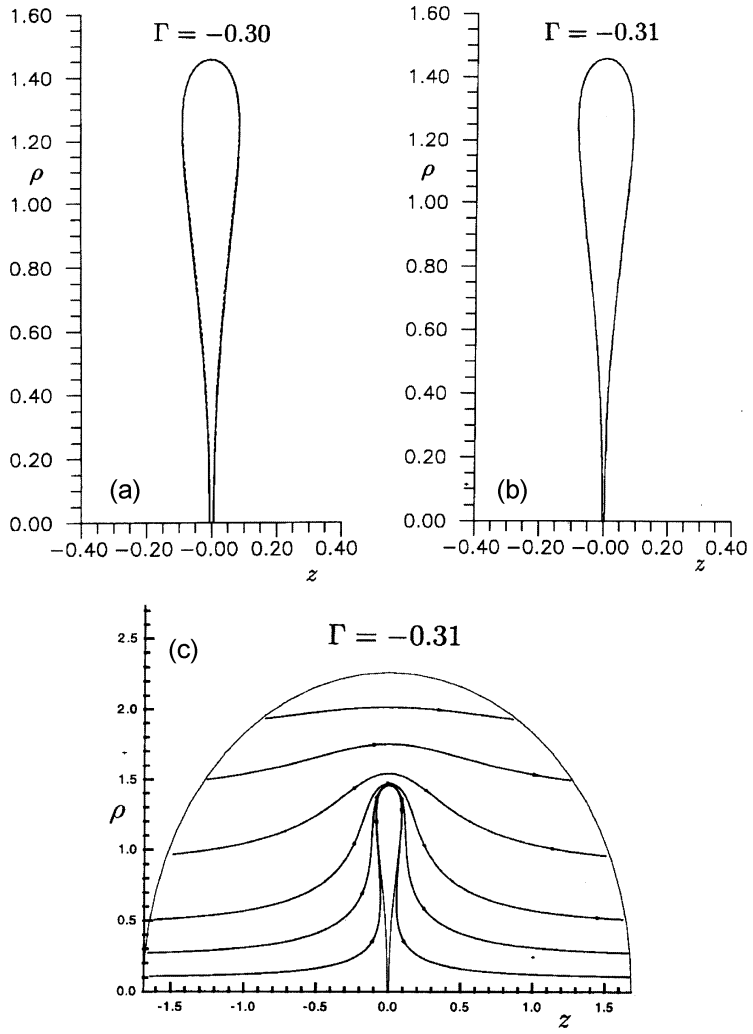

Figure 8. Bubble shapes in the neighbourhood of pinch-off, $\Gamma \to \Gamma^*$. (**a**) $m = 20$, (- - -) $n = 300$, (– – –) $n = 460$, $n = 600$ (—). (**b**) $m = 25$, $n = 600$. (**c**) Streamlines in the meridional plane for $\Gamma = -0.31$.

bubble shape, such as the present ones and MVK, can yield very similar W–χ plots with the expected maxima and as a consequence this plot cannot be used to determine the correctness or otherwise of a calculation. The power dependence in (15) contributes greatly to this insensitivity. Also note that even though the two-point approximation is a poor one as shown in §3, it does yield a maximum W. This, we believe, explains why it is referred to so much more often than the excellent linearized approximation (12), which does not yield a maximum W.

The W–χ plot is also responsible, we believe, for the failure of previous workers to detect the errors in MVK inspite of the many citations to it. Instead of computing

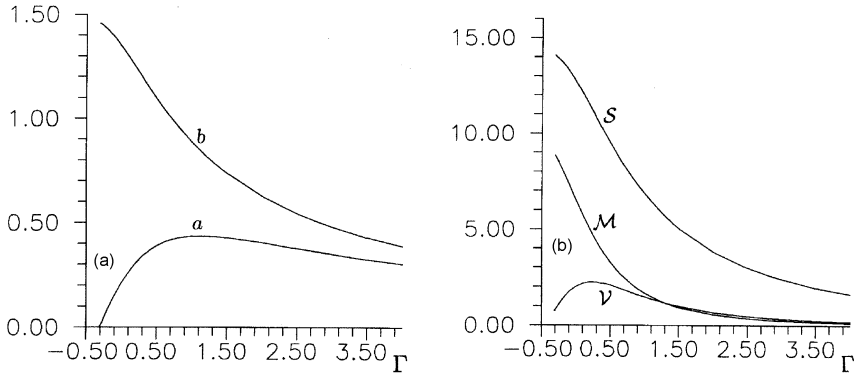

Figure 9. Bubble parameters as functions of Γ for $\Gamma \leq 4$. (**a**) The streamwise (a) and transverse (b) dimensions. (**b**) The surface area $\mathcal{S}$, volume $\mathcal{V}$ and added mass $\mathcal{M}$.

and comparing bubble shapes at the odd values of Γ chosen by MVK, most papers just compute the above plot and claim agreement with MVK. Ryskin and Leal [26] refer almost exclusively to this aspect when citing MVK but no detailed comparisons are made since their computations are for $\mathrm{Re} \leq 200$. However in Ryskin and Leal [26] which deals with straining flows, they consider the inviscid limit and compare their results with those of Miksis [27] and claim good agreement based on $\mathrm{W_c}$ alone. Meiron [13] plots the equivalent of the W–χ plot and then says "It can be seen in agreement with the results of Miksis *et al* [1], Moore [11] and El Sawi [21] that the Weber number has a broad maximum at $We = 1.27$." Similarly in Pozrikidis [14], after giving a similar plot, we find "Our results are in perfect agreement with the numerical calculations presented by the last authors (MVK)." More recently Séro-Guillaume and Er-Riani [28] compare their results with those of MVK and conclude "we notice that they obtained more elongated shapes", a polite way of saying that there was disagreement. But again like earlier authors they claimed good agreement based on the maximum Weber number. All these point out to the importance of dealing directly with bubble shapes rather than with parameters deduced from them, especially the Weber number.

We conclude by pointing out that the geometrical and dynamical parameters discussed above have been listed in table 3 as functions of Γ for the range $-0.31 \leq \Gamma \leq 1000$. Thus between table 2, which lists the bubble mapping coefficients, and table 3, anyone can compute bubble parameters over the whole range of Γ either by interpolation or directly from the bubble shape.

6. Conclusion

We have in this paper presented a method for computing axisymmetric, inviscid bubble shapes over the whole range of Γ that is simple, rugged, reasonably accurate and fast. However, the greatest merit of this method is that bubble shapes are described analytically by a mapping that is very well-suited to these shapes. As a consequence it will be possible to both check and easily use the shapes and

Table 3. Bubble parameters as functions of Γ.

Γ	a	b	$\mathcal{S}$	$\mathcal{V}$	$\mathcal{M}$
1000.00	0.00200	0.00200	0.50116E−04	0.33361E−07	0.16751E−07
100.00	0.01956	0.01978	0.48790E−02	0.32045E−04	0.16280E−04
90.00	0.02168	0.02195	0.60041E−02	0.43745E−04	0.22312E−04
80.00	0.02431	0.02465	0.75678E−02	0.61902E−04	0.31632E−04
70.00	0.02768	0.02812	0.98326E−02	0.91675E−04	0.46957E−04
60.00	0.03212	0.03272	0.13290E−01	0.14405E−03	0.74017E−04
50.00	0.03826	0.03912	0.18951E−01	0.24529E−03	0.12659E−03
40.00	0.04731	0.04863	0.29181E−01	0.46864E−03	0.24345E−03
30.00	0.06194	0.06425	0.50639E−01	0.10711E−02	0.56249E−03
20.00	0.08963	0.09465	0.10862E+00	0.33637E−02	0.18045E−02
10.00	0.16145	0.17957	0.37830E+00	0.21812E−01	0.12444E−01
9.00	0.17531	0.19721	0.45308E+00	0.28570E−01	0.16477E−01
8.00	0.19178	0.21873	0.55264E+00	0.38450E−01	0.22539E−01
7.00	0.21154	0.24550	0.68883E+00	0.53435E−01	0.31971E−01
6.00	0.23560	0.27970	0.88198E+00	0.77265E−01	0.47480E−01
5.00	0.26534	0.32489	0.11685E+01	0.11745E+00	0.74832E−01
4.00	0.30257	0.38731	0.16188E+01	0.19047E+00	0.12779E+00
3.00	0.34905	0.47888	0.23822E+01	0.33635E+00	0.24446E+00
2.00	0.40287	0.62498	0.38124E+01	0.66358E+00	0.55460E+00
1.50	0.42637	0.73494	0.50242E+01	0.97547E+00	0.91690E+00
1.00	0.43348	0.88604	0.68243E+01	0.14563E+01	0.16475E+01
0.80	0.42523	0.96194	0.77696E+01	0.16975E+01	0.21377E+01
0.60	0.40521	1.04801	0.88627E+01	0.19454E+01	0.28128E+01
0.40	0.36759	1.14392	0.10095E+02	0.21517E+01	0.37387E+01
0.20	0.30506	1.24653	0.11416E+02	0.22189E+01	0.49750E+01
0.00	0.21138	1.34529	0.12674E+02	0.19928E+01	0.64670E+01
−0.05	0.18251	1.36829	0.12964E+02	0.18718E+01	0.68749E+01
−0.10	0.15151	1.38985	0.13234E+02	0.17209E+01	0.72841E+01
−0.15	0.11839	1.40969	0.13480E+02	0.15384E+01	0.76889E+01
−0.20	0.08305	1.42744	0.13696E+02	0.13230E+01	0.80815E+01
−0.25	0.04472	1.44292	0.13881E+02	0.10691E+01	0.84588E+01
−0.26	0.03628	1.44580	0.13915E+02	0.10110E+01	0.85344E+01
−0.27	0.02735	1.44861	0.13947E+02	0.94886E+00	0.86102E+01
−0.28	0.02127	1.45000	0.13964E+02	0.91243E+00	0.86627E+01
−0.29	0.01420	1.45293	0.14004E+02	0.86131E+00	0.87433E+01
−0.30	0.00636	1.45582	0.14042E+02	0.80416E+00	0.87994E+01
−0.31	0.00332	1.45788	0.14065E+02	0.75856E+00	0.88426E+01

parameters presented here in tables 2 and 3. A by-product of the present work is that some errors in an earlier work have been found and corrected. We have also shown that Moore's linearized result for large Γ is an excellent approximation up to quite low values of the parameter. This result should be useful in the approximate calculation of inviscid bubble shapes.

Acknowledgement

I would like to thank my colleague, C L Narayana, for introducing me to the panel method, my wife, Priti Shankar, for valuable advice on the presentation of this paper and D Shobha for help in preparing the manuscript.

References

[1] M Miksis, J-M Vanden-Broeck and J B Keller, *J. Fluid Mech.* **18**, 89 (1981)
[2] W L Haberman and R K Morton, *Proc. ASCE* **387**, 227 (1954)
[3] D W Moore, *J. Fluid Mech.* **6**, 113 (1959)
[4] R C Clift, J R Grace and M E Weber, *Bubbles, drops and particles* (Academic Press, 1978)
[5] D Bhaga and M E Weber, *J. Fluid Mech.* **105**, 61 (1981)
[6] J Magnaudet and I Eames, *Annu. Rev. Fluid Mech.* **32**, 659 (2000)
[7] R A Hartunian and W R Sears, *J. Fluid Mech.* **3**, 27 (1957)
[8] P C Duineveld, *J. Fluid Mech.* **292**, 325 (1995)
[9] V G Levich, *Physicochemical hydrodynamics* (Prentice-Hall, Englewood Cliffs, N.J., 1962)
[10] D W Moore, *J. Fluid Mech.* **16**, 161 (1963)
[11] D W Moore, *J. Fluid Mech.* **23**, 749 (1965)
[12] G Ryskin and L G Leal, *J. Fluid Mech.* **148**, 37 (1984)
[13] D I Meiron, *J. Fluid Mech.* **198**, 101 (1989)
[14] C Pozrikidis, *J. Fluid Mech.* **209**, 77 (1989)
[15] P N Shankar, *J. Fluid Mech.* **244**, 187 (1992)
[16] J L Hess and A M O Smith, *Prog. Aero. Sci.* **8**, 1 (1967)
[17] The formula for the curvature given in Christov and Volkov [18] is in general incorrect. However, the author does not know whether this invalidates any of their results
[18] C I Christov and P K Volkov, *J. Fluid Mech.* **158**, 341 (1985)
[19] Because MVK do not provide numerical data we have had to scan their figures and deduce pointwise coordinates for sample points. This leads to some inaccuracy. Another source is from the fact that their figures do not have accurate fore-aft symmetry; in correspondence, Prof Miksis explained that the figures were hand-drawn with the curves in three of the quadrants reflected from those in the first
[20] Till now an unsuspecting reader who read MVK's statement "For $\gamma > 4$ our results agree with Moore's (1965) results within 10%" would have concluded that something was wrong with Moore's results, since one would expect a full non-linear calculation to be very accurate. In fact it is the other way around
[21] M El Sawi, *J. Fluid Mech.* **62**, 163 (1974)
[22] E B McLeod, *J. Rat. Mech. Anal.* **4**, 557 (1955)
[23] C S Yih, *Fluid mechanics* (McGraw-Hill, 1969)
[24] J N Newman, *Marine hydrodynamics* (MIT Press, 1977)
[25] In this connection two observations made by Ryskin and Leal [26] are pertinent. First, the existence of steady solutions for $W < W_c$ is no guarantee of their stability. Second, the need to distinguish 'shape instability', which is considered here, with 'path instability', which cannot be predicted by axisymmetric analyses. In fact, Ryskin and Leal express the opinion that the close agreement seen between the inviscid results for W_c and the critical value observed in experiments for path instability is purely coincidental!
[26] G Ryskin and L G Leal, *J. Fluid Mech.* **148**, 19 (1984)
[27] M Miksis, *Phys. Fluids* **24**, 1229 (1981)
[28] O Séro-Guillaume and M Er-Riani, *Euro. J. Mech. B/Fluids* **18**, 991 (1999)